Variable Conduction Mode Control Method to Reduce Torque Ripple for Symmetrical Winding Multiphase Brushless DC Motor

Wei Chen, *Member, IEEE*, Lixiang Zhu, Xinmin Li, *Member, IEEE*, Zhiqiang Wang, *Member, IEEE*, Chen Li, and Tingna Shi, *Senior Member, IEEE*

***Abstract*—Increasing the number of phases in a motor can enhance control freedom, offering more possibilities for high-performance motor drives. For the symmetrical winding multiphase brushless dc motor (BLDCM), this article proposes a variable conduction mode control method to reduce torque ripple. The proposed method divides the torque intervals based on two types of constraints: 1) equal copper loss and 2) equal phase current amplitude. It utilizes the torque reference value to identify the torque interval and selects the conduction mode that minimizes torque ripple within that interval. During motor operation, the conduction mode can be dynamically switched with load variations. By optimally arranging and combining different conduction modes based on the motor's torque output characteristics, this method significantly reduces torque ripple within each torque interval. This method does not require additional hardware circuits in general multiphase motor systems, making it simple and easy to implement. The validity of the proposed method is verified through experiments using a nine-phase BLDCM as a prototype.**

***Index Terms*—Multiphase brushless dc motor (BLDCM), output torque, torque ripple, variable conduction mode.**

I. Introduction

IN RECENT years, with the development of high-performance rare-earth permanent magnet materials and low-cost power electronic devices, permanent magnet motors have been widely used in household, medical, and transportation fields [1], [2]. Due to their high power density, high efficiency, and excellent dynamic performance, permanent magnet motors are also becoming increasingly popular in low-voltage, high-power applications such as electric vehicles, more-electric aircraft, and marine propulsion [3], [4].

Permanent magnet motors are generally classified into permanent magnet synchronous motors (PMSMs) and brushless dc motors (BLDCMs). In principle, the torque density of BLDCMs is 15% higher than that of PMSMs because their trapezoidal air gap flux more fully utilizes the stator core material [5], [6]. However, the torque ripple has always been a major factor hindering the high-performance drive of BLDCMs.

Currently, in terms of motor control, there are three main categories of control methods for suppressing torque ripple: 1) adding dc–dc converter topologies [7], [8], [9], 2) modifying modulation strategies [10], [11], [12], [13], and 3) changing control strategies [14], [15], [16].

Methods that involve adding dc–dc converter topologies generally use boosting to maintain the stability of the noncommutating current during commutation, thereby reducing commutation torque ripple. Based on the Z-source inverter in [7], the shoot-through vector is introduced to increase the dc-link voltage, and the stability of the noncommutating current is maintained by adjusting the duty cycles of the shoot-through vector and active vector. A noninductive boost front-end topology is used in [8], which utilizes the motor stator inductance to boost the capacitor to meet the voltage requirements during commutation. Based on the diode-assisted buck–boost inverter in [9], four types of switching vectors are constructed according to the motor's operating modes. By reasonably designing the duration and sequence of the switching vectors, commutation torque ripple can be reduced across the entire speed range.

For methods that modify modulation strategies, torque ripple caused by current commutation or pulsewidth modulation (PWM) chopping can be reduced. An improved three-phase modulation strategy is proposed in [10], aiming to optimize the current slope by using phase voltage and back electromotive force (EMF) at the start and end of the commutation region, combined with a voltage compensation method to reduce commutation torque ripple. The delay in PWM and its effects are analyzed in [11], which synchronizes the commutation cycle with the switching cycle, effectively maintaining the minimum commutation cycle and minimizing commutation torque ripple in low-inductance BLDCM. The relationship between PWM frequency and torque ripple is analyzed in [12], confirming that

Received 27 May 2024; revised 31 August 2024; accepted 29 September 2024. Date of publication 3 October 2024; date of current version 12 December 2024. This work was supported in part by the National Natural Science Foundation of China under Grant 52077156 and in part by the Zhejiang Provincial Natural Science Foundation of China under Grant LD24E070001. Recommended for publication by Associate Editor R. Kennel. *(Corresponding author: Xinmin Li.)*

Wei Chen, Xinmin Li, and Zhiqiang Wang are with the School of Electrical Engineering, Tiangong University, Tianjin 300387, China (e-mail: chen_wei@tiangong.edu.cn; lixinmin@tju.edu.cn; wangzhiqiang@tiangong.edu.cn).

Lixiang Zhu is with the School of Control Science and Engineering, Tiangong University, Tianjin 300387, China (e-mail: 1931065391@tiangong.edu.cn).

Chen Li is with the Zhejiang University Advanced Electrical Equipment Innovation Center, Hangzhou 311107, China (e-mail: lichen_hz@zju.edu.cn).

Tingna Shi is with the College of Electrical Engineering, Zhejiang University, Hangzhou 310027, China, and also with the Zhejiang University Advanced Electrical Equipment Innovation Center, Hangzhou 311107, China (e-mail: tnshi@zju.edu.cn).

Color versions of one or more figures in this article are available at https://doi.org/10.1109/TPEL.2024.3472644.

Digital Object Identifier 10.1109/TPEL.2024.3472644

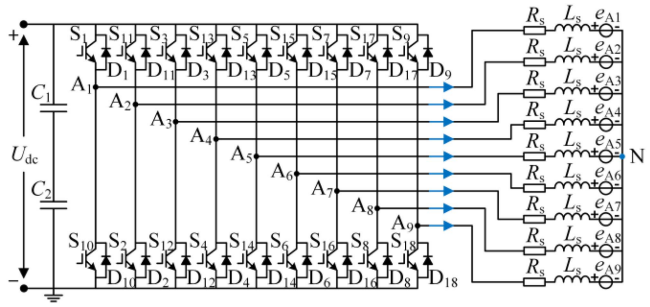

Fig. 1. Equivalent circuit of the nine-phase BLDCM drive system.

increasing the PWM frequency at the same speed can improve current waveform quality and reduce torque ripple caused by PWM chopping. Different modulation methods and their corresponding torque ripples are compared in [13], which proposes an improved modulation strategy called PWM-ON-PWM, although the reduction in PWM torque ripple is minimal.

For methods that change control strategies, torque is generally used as the control target to reduce torque ripple caused by nonideal back-EMF. A torque control method is proposed in [14], which designs current control rules to reduce torque ripple by measuring the waveform function of the back-EMF and adjusting the PWM duty cycle in real-time. Two switching tables with the main vector and subsidiary vector are established for both the normal conduction period and the commutation period of the motor in [15]. Combining the main and subsidiary vectors within each control cycle allows the torque ripple caused by nonideal back-EMF and current commutation to be simultaneously reduced. The output modes of the Cuk converter are restructured in [16], which adopts the concept of average torque control during the motor's normal conduction period to reduce torque ripple by reasonably controlling the inverter's PWM duty cycle.

The torque ripple suppression methods mentioned above are all based on three-phase BLDCM systems and have been proven effective. However, for low-voltage and high-power applications of multiphase BLDCM systems, most of these methods are hard for transfer and application. For example, adding dc–dc converter topologies would increase the size and cost of the general system, which is a significant problem for multiphase BLDCM systems. Modifying modulation strategies would greatly increase the complexity of multiphase control. Nevertheless, changing control strategies holds significant research potential. This is because increasing the number of phases in a multiphase motor enhances the freedom of control, providing more possibilities for high-performance motor drives.

The symmetrical winding multiphase BLDCM has the characteristic of flexible conduction, allowing for different conduction mode controls. Two types of parallel multiphase BLDCMs are compared and analyzed in [17], using a nine-phase motor as an example to demonstrate the operating characteristics of the symmetrical winding multiphase BLDCM under different conduction modes and deriving the output torque comparison relationships. However, the literature did not analyze the torque ripple corresponding to different conduction modes. Through further research, this article finds that under the same speed and load torque conditions, the torque ripple caused by PWM

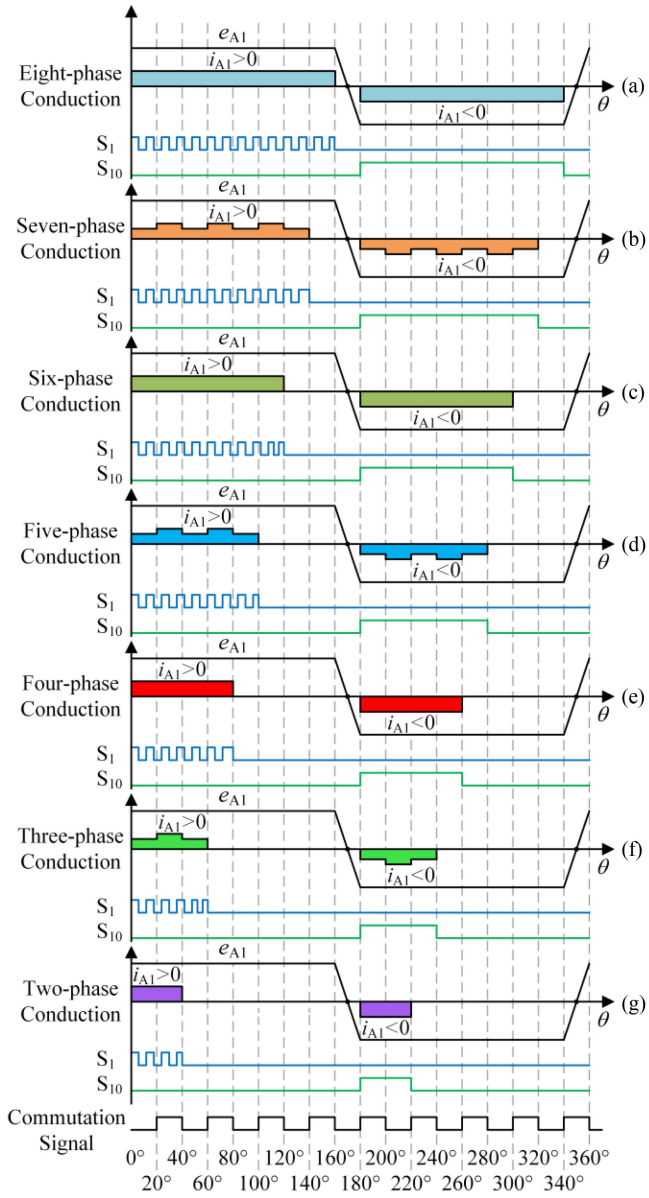

Fig. 2. Phase relationship between the back-EMF and the current of phase A_1 for the nine-phase BLDCM under different conduction modes. (a)–(g) Eight-phase to two-phase windings conduction.

chopping in symmetrical winding multiphase BLDCM varies with different conduction modes. The observed phenomenon is that the torque ripple gradually decreases as the number of conducting phases is reduced. This finding provides a new solution for achieving low torque ripple operation in symmetrical winding multiphase BLDCM drive systems.

This article analyzes the torque output characteristics of symmetrical winding multiphase BLDCM and proposes a variable conduction mode control method. The proposed method uses equal copper loss and equal phase current amplitude as two kinds of constraints to divide the torque into intervals. It utilizes the torque reference value to identify the torque interval and selects the conduction mode that minimizes torque ripple within that interval. This method fully exploits the operating characteristics of symmetrical winding multiphase BLDCM, enabling optimized control of both output torque and torque ripple.

The rest of this article is organized as follows. Section II describes the mathematical model and conduction mode of symmetrical winding multiphase BLDCM and compares the output torque between different conduction modes. Section III analyzes the torque ripple corresponding to different conduction modes and introduces the proposed variable conduction mode control method. Section IV conducts experimental validation and analysis. Finally, Section V concludes this article.

II. Operation Characteristics of Symmetrical Winding Multiphase BLDCM

A. Mathematical Model and Conduction Mode

The armature windings of a symmetrical winding multiphase BLDCM are uniformly distributed in space and have only one neutral point. Taking a nine-phase BLDCM as an example, the motor and its drive system can be simplified to the equivalent circuit, as shown in Fig. 1, where the multiphase motor is modeled as resistance, inductance, and back-EMF connected in series.

As shown in Fig. 1, each phase armature winding is connected to the midpoint of the inverter bridge arm, with the number of windings equaling the number of bridge arms. Where U_{dc} represents the dc-bus voltage, C_1–C_2 are the filtering capacitors, S_1–S_{18} are the power switching devices, D_1–D_{18} are the freewheeling diodes, A_1–A_9 are the phase windings, R_{s} is the phase resistance, L_{s} is the phase inductance, $e_{\mathrm{A}1}$–$e_{\mathrm{A}9}$ are the phase back-EMFs, and N is the neutral point.

According to the system equivalent circuit shown in Fig. 1, the voltage equation of the symmetrical winding multiphase BLDCM can be expressed as

$$\begin{cases} u_{\mathrm{A}1} = R_{\mathrm{s}} i_{\mathrm{A}1} + L_{\mathrm{s}} \frac{\mathrm{d}i_{\mathrm{A}1}}{\mathrm{d}t} + e_{\mathrm{A}1} + u_{\mathrm{N}} \\ u_{\mathrm{A}2} = R_{\mathrm{s}} i_{\mathrm{A}2} + L_{\mathrm{s}} \frac{\mathrm{d}i_{\mathrm{A}2}}{\mathrm{d}t} + e_{\mathrm{A}2} + u_{\mathrm{N}} \\ u_{\mathrm{A}3} = R_{\mathrm{s}} i_{\mathrm{A}3} + L_{\mathrm{s}} \frac{\mathrm{d}i_{\mathrm{A}3}}{\mathrm{d}t} + e_{\mathrm{A}3} + u_{\mathrm{N}} \\ \quad \vdots \\ u_{\mathrm{A}(m-1)} = R_{\mathrm{s}} i_{\mathrm{A}(m-1)} + L_{\mathrm{s}} \frac{\mathrm{d}i_{\mathrm{A}(m-1)}}{\mathrm{d}t} + e_{\mathrm{A}(m-1)} + u_{\mathrm{N}} \\ u_{\mathrm{A}m} = R_{\mathrm{s}} i_{\mathrm{A}m} + L_{\mathrm{s}} \frac{\mathrm{d}i_{\mathrm{A}m}}{\mathrm{d}t} + e_{\mathrm{A}m} + u_{\mathrm{N}} \end{cases} \tag{1}$$

where $u_{\mathrm{A}1}$~$u_{\mathrm{A}m}$ are the phase voltages, $i_{\mathrm{A}1}$~$i_{\mathrm{A}m}$ are the phase currents, u_{N} is the neutral point voltage, and m is the number of phases (with m being an odd number).

The armature windings are connected in a star configuration. According to Kirchhoff's current law, the phase currents satisfy the following relationship as:

$$i_{\mathrm{A}1} + i_{\mathrm{A}2} + i_{\mathrm{A}3} + \cdots + i_{\mathrm{A}(m-1)} + i_{\mathrm{A}m} = 0. \tag{2}$$

The converted electromagnetic power acts on the load in the form of torque. Under ideal conditions, the electromagnetic torque equation can be expressed as

$$P_{\mathrm{e}} = T_{\mathrm{e}}\omega \tag{3}$$

$$T_{\mathrm{e}} = \frac{e_{\mathrm{A}1}i_{\mathrm{A}1} + e_{\mathrm{A}2}i_{\mathrm{A}2} + e_{\mathrm{A}3}i_{\mathrm{A}3} + \cdots + e_{\mathrm{A}(m-1)}i_{\mathrm{A}(m-1)} + e_{\mathrm{A}m}i_{\mathrm{A}m}}{\omega} \tag{4}$$

where ω represents the mechanical angular velocity.

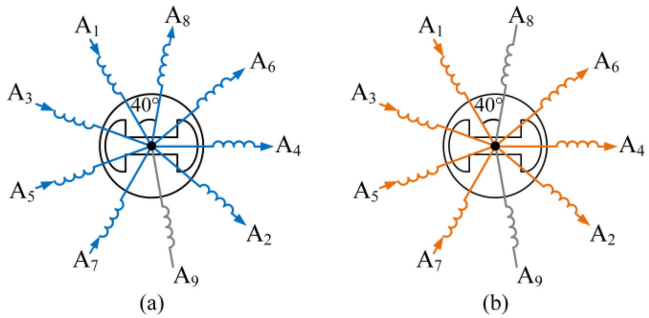

Fig. 3. Conduction results of the armature winding in the first sector of the nine-phase BLDCM. (a) Eight-phase conduction mode. (b) Seven-phase conduction mode.

As the number of phases in a symmetrical winding multiphase BLDCM increases, a larger flat-top width of the back-EMF is required to fully utilize each phase winding and achieve a smooth output torque. Generally, in the design of a m-phase BLDCM, the flat-top width W of the back-EMF follows the relationship as

$$W = \frac{m-1}{m}\pi. \tag{5}$$

The broad flat-topped region of the back EMF provides a foundation for changing the conduction mode of the windings. Additionally, as the number of motor phases increases, the rotor position sectors are divided into smaller segments, allowing for more flexible control methods if the winding conduction modes are changed.

For a m-phase BLDCM, if the control method of conducting all m-phase windings is used and the square wave current is applied, periodic torque ripple will occur due to the insufficient width of the back-EMF flat-top region. Additionally, special commutation points are required, so this method is not used to control the motor in this article. Furthermore, if the control methods of conducting (m–1)-phase, (m–3)-phase, and (m–5) phase windings are adopted, it is called even-phase winding conduction. If the control methods of conducting (m–2)-phase, (m–4)-phase, and (m–6)-phase windings are adopted, it is called odd-phase winding conduction. Taking $m = 9$ as an example, as shown in Fig. 2, it illustrates the phase relationship between the back-EMF and the current of phase A_1 when different conduction modes are used in a nine-phase BLDCM. Fig. 2(a)–(g), respectively, shows the conduction of eight-phase to two-phase windings.

As shown in Fig. 2, when controlling the nine-phase BLDCM, the entire electrical cycle is divided into 18 sectors, with the motor commutating every 20 electrical degrees. When using the traditional H_PWM-L_ON modulation strategy, the upper bridge power switching devices corresponding to each phase winding perform PWM chopping within the conducting sector. In contrast, the lower bridge switching devices remain continuously on. For example, S_1 performs PWM chopping, and S_{10} remains continuously on for phase A_1. The difference between conduction modes lies in the number of armature windings simultaneously conducting within each sector, but the pulse generation method for the power switching devices S_1–S_{18} is the same.

As shown in Fig. 3, it depicts the armature winding conduction results in the first sector (0–20°) of the nine-phase BLDCM,

using eight-phase and seven-phase conduction modes as examples. For different conduction modes, floating phases are set according to the number of armature windings that need to be energized, allowing each phase to be sequentially floated throughout the entire electrical cycle. In different conduction modes, conduction begins at the start of the back-EMF flat-top region to accurately utilize the commutation points based on the Hall signals.

B. Output Torque Comparison Between Different Conduction Modes

Due to its inherent flexibility, the symmetrical winding multiphase BLDCM can be controlled using different conduction modes. However, to ensure the safety and stable operation of the motor system, it is necessary to constrain the current. Therefore, the output torque corresponding to different conduction modes varies. This section analyzes the comparative relationship between the average torques of different conduction modes using copper loss and phase current amplitude as constraint conditions.

When the *m*-phase BLDCM is controlled using the (*m*–1)-phase conduction mode, the steady-state electromagnetic power equation can be expressed as

$$P_{\mathrm{e\_}(m-1)} = (m-1)EI_{(m-1)} \tag{6}$$

where E is the amplitude of the back-EMF, and $I_{(\mathrm{m\text{-}1})}$ is the amplitude of the phase current.

According to $E = k_{\mathrm{e}}\omega$, by substituting (6) into (4), the average torque equation can be obtained as

$$T_{\mathrm{e\_}(m-1)} = (m-1)k_{\mathrm{e}}I_{(m-1)} \tag{7}$$

where k_{e} is the coefficient of the back-EMF.

When the *m*-phase BLDCM is controlled by (*m*–2)-phase conduction mode, the average torque equation can be written as

$$T_{\mathrm{e\_}(m-2)} = \frac{(m-1)}{2}k_{\mathrm{e}}I_{(m-2)\_\mathrm{up}} + \frac{(m-3)}{2}k_{\mathrm{e}}I_{(m-2)\_\mathrm{down}}. \tag{8}$$

From (8), it is known that the average torque equation of the motor under the odd-number phase conduction mode consists of two parts. Since the number of armature windings that are simultaneously energized with the positive pole of the power supply differs from those energized with the negative pole within each sector, $I_{(m\text{-}2)\_\mathrm{up}} \neq I_{(m\text{-}2)\_\mathrm{down}}$. However, the neutral point current satisfies Kirchhoff's current law, from which it can be derived that $I_{(m\text{-}2)\_\mathrm{up}} / I_{(m\text{-}2)\_\mathrm{down}} = (m\text{-}3) / (m\text{-}1)$.

In the conduction modes of the (*m*–1)-phase and (*m*–2)-phase, the copper losses of the motor windings can be, respectively, represented as

$$\begin{cases} P_{\mathrm{Cu\_}(m-1)} = mR_{\mathrm{s}}I^2_{\mathrm{rms\_}(m-1)} \\ P_{\mathrm{Cu\_}(m-2)} = mR_{\mathrm{s}}I^2_{\mathrm{rms\_}(m-2)} \end{cases} \tag{9}$$

where I_{rms} is the root mean square (rms) value of the phase current.

When the constraint condition of equal copper losses is satisfied, i.e., $P_{\mathrm{Cu\_}(m\text{-}1)} = P_{\mathrm{Cu\_}(m\text{-}2)}$, the following can be obtained as:

$$\frac{I_{\mathrm{rms\_}(m-1)}}{I_{\mathrm{rms\_}(m-2)}} = 1. \tag{10}$$

The relationship between the rms value and the amplitude of the phase current varies depending on the conduction mode. When the *m*-phase BLDCM adopts the (*m*–1)-phase and (*m*–2)-phase conduction modes, the relationship between the two can be expressed as

$$I_{\mathrm{rms\_}(m-1)} = \sqrt{\frac{m-1}{m}}I_{(m-1)} \tag{11}$$

$$\begin{cases} I_{\mathrm{rms\_}(m-2)\_\mathrm{up}} = \sqrt{\frac{(m-2)(m-1)}{m(m-3)}}I_{(m-2)\_\mathrm{up}} \\ I_{\mathrm{rms\_}(m-2)\_\mathrm{down}} = \sqrt{\frac{(m-2)(m-3)}{m(m-1)}}I_{(m-2)\_\mathrm{down}}. \end{cases} \tag{12}$$

By substituting (10) into (11) and (12), the comparative relationship of the phase current amplitudes can be derived as

$$\begin{cases} \frac{I_{(m-1)}}{I_{(m-2)\_\mathrm{up}}} = \sqrt{\frac{m-2}{m-3}} \\ \frac{I_{(m-1)}}{I_{(m-2)\_\mathrm{down}}} = \sqrt{\frac{(m-2)(m-3)}{m-1}}. \end{cases} \tag{13}$$

Furthermore, by substituting (13) into (7) and (8), the comparative relationship of the average torque can be derived as

$$\begin{cases} \frac{T_{\mathrm{e\_}(m-1)}}{T_{\mathrm{e\_}(m-2)\_\mathrm{up}}} = \sqrt{\frac{m-2}{m-3}} \\ \frac{T_{\mathrm{e\_}(m-1)}}{T_{\mathrm{e\_}(m-2)\_\mathrm{down}}} = \sqrt{\frac{m-2}{m-3}}. \end{cases} \tag{14}$$

From (14), it can be seen that the two different phase current expressions in (12) yield the same comparative relationship for average torque. For the *m*-phase BLDCM, using the (*m*–1)-phase conduction mode control produces a higher output torque than using the (*m*–2)-phase conduction mode.

Following the abovementioned analysis process, the average torque for other conduction modes can be derived. Table I presents the comparative relationship of average torque between adjacent conduction modes for the *m*-phase BLDCM under the constraint of equal copper losses.

TABLE I
COMPARISON OF AVERAGE TORQUE BETWEEN ADJACENT CONDUCTION MODES WITH EQUAL COPPER LOSS AS THE CONSTRAINT

$\frac{T_{\mathrm{e\_}(m-1)}}{T_{\mathrm{e\_}(m-2)}}$	$\frac{T_{\mathrm{e\_}(m-2)}}{T_{\mathrm{e\_}(m-3)}}$	$\frac{T_{\mathrm{e\_}(m-3)}}{T_{\mathrm{e\_}(m-4)}}$	$\frac{T_{\mathrm{e\_}(m-4)}}{T_{\mathrm{e\_}(m-5)}}$	$\frac{T_{\mathrm{e\_}(m-5)}}{T_{\mathrm{e\_}(m-6)}}$	$\frac{T_{\mathrm{e\_}(m-6)}}{T_{\mathrm{e\_}(m-7)}}$
$\sqrt{\frac{m-2}{m-3}}$	$\sqrt{\frac{m-1}{m-2}}$	$\sqrt{\frac{m-4}{m-5}}$	$\sqrt{\frac{m-3}{m-4}}$	$\sqrt{\frac{m-6}{m-7}}$	$\sqrt{\frac{m-5}{m-6}}$

When comparing the average torque under the constraint of equal phase current amplitudes, it can be seen from (8) that $I_{(m\text{-}2)\_\mathrm{down}} > I_{(m\text{-}2)\_\mathrm{up}}$. Therefore, let $I_{(m\text{-}2)\_\mathrm{down}} = I_{(m\text{-}1)}$, and the following can be obtained as:

$$\frac{T_{\mathrm{e\_}(m-1)}}{T_{\mathrm{e\_}(m-2)}} = \frac{m-1}{m-3}. \tag{15}$$

From (15), it can be seen that for the *m*-phase BLDCM, using the (*m*–1)-phase conduction mode produces a higher output

TABLE II
COMPARISON OF AVERAGE TORQUE BETWEEN ADJACENT CONDUCTION MODES WITH EQUAL PHASE CURRENT AMPLITUDE AS THE CONSTRAINT

$\frac{T_{e\_(m-1)}}{T_{e\_(m-2)}}$	$\frac{T_{e\_(m-2)}}{T_{e\_(m-3)}}$	$\frac{T_{e\_(m-3)}}{T_{e\_(m-4)}}$	$\frac{T_{e\_(m-4)}}{T_{e\_(m-5)}}$	$\frac{T_{e\_(m-5)}}{T_{e\_(m-6)}}$	$\frac{T_{e\_(m-6)}}{T_{e\_(m-7)}}$
$\frac{m-1}{m-3}$	1	$\frac{m-3}{m-5}$	1	$\frac{m-5}{m-7}$	1

torque than using the (m–2)-phase conduction mode. Similarly, as shown in Table II, the comparative relationship of average torque between adjacent conduction modes can be derived under the constraint of equal phase current amplitudes.

By observing Tables I and II, it can be seen that the comparative results of average torque between adjacent conduction modes are greater than or equal to 1 under the constraints of equal copper losses and equal phase current amplitudes. Therefore, the theoretical analysis indicates that the torque output capability of a symmetrical winding multiphase BLDCM gradually decreases as the number of conducting phases diminishes under current constraint conditions. When the load torque varies, it is necessary to switch conduction modes to ensure torque output performance dynamically.

III. Optimal Control Strategy of Symmetrical Winding Multiphase BLDCM

Under current constraints, the output torque of a symmetrical winding multiphase BLDCM varies with different conduction modes. Further research in this article reveals that the torque ripple corresponding to different conduction modes also varies under the same speed and load torque conditions. Specifically, the torque ripple decreases as the number of conducting phases reduces. Therefore, this article proposes a variable conduction mode control method. This method divides the torque intervals based on the torque output capabilities of different conduction modes and uses the torque reference value to identify the torque interval. By dynamically switching the conduction mode according to load changes, we can achieve low torque ripple operation in symmetrical winding multiphase BLDCM drive systems.

A. Torque Ripple Analysis Under Different Conduction Modes

The symmetrical winding multiphase BLDCM typically uses PWM for control during the driving process. However, the presence of inductance in the phase windings leads to current fluctuations due to PWM chopping, which in turn causes electromagnetic torque ripples at the same frequency. Fig. 4 displays the phase current and electromagnetic torque waveforms within each PWM cycle. This section uses a nine-phase BLDCM as an example to analyze the variation in torque ripples when controlled using different conduction modes.

1) Torque Ripple During Normal Conduction Period: As shown in Fig. 5, they are the system equivalent circuits of the nine-phase BLDCM when operating in the eight-phase conduction mode, where Fig. 5(a) and (b), respectively, show the

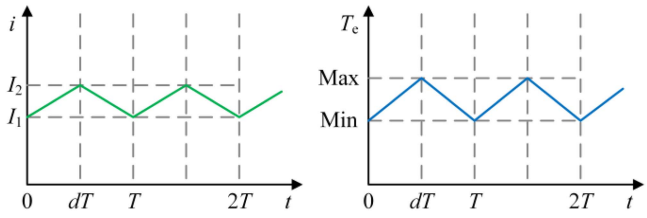

Fig. 4. Phase current and electromagnetic torque waveforms within each PWM cycle.

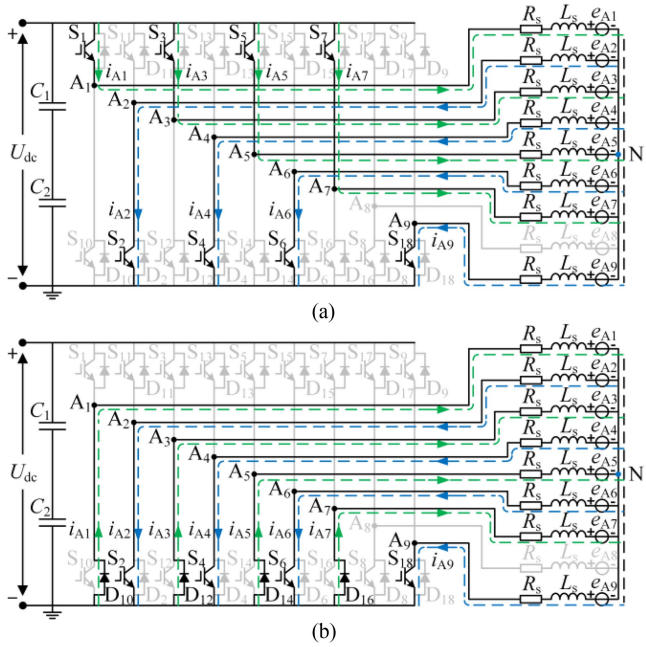

Fig. 5. System equivalent circuits of the nine-phase BLDCM with eight-phase conduction during the normal conduction period within one PWM cycle. (a) PWM = ON. (b) PWM = OFF.

current flow paths when PWM = ON and PWM = OFF within one switching cycle during the normal conduction period.

For the eight-phase conduction mode, the H_PWM-L_ON modulation strategy is used as an example. From Fig. 5(a), it can be observed that when PWM is ON, current flows into the windings of phases A_1, A_3, A_5, and A_7 from the positive terminal of the power supply and flows out from the windings of phases A_2, A_4, A_6, and A_9, forming a closed circuit through the negative terminal of the power supply. The winding of phase A_8 is a floating phase, with no current passing through. The corresponding voltage equation is

$$\begin{cases} u_{Ax} = U_{dc} = R_s i_{Ax} + L_s \frac{di_{Ax}}{dt} + e_{Ax} + u_N \\ u_{Ay} = 0 = R_s i_{Ay} + L_s \frac{di_{Ay}}{dt} + e_{Ay} + u_N \end{cases} \tag{16}$$

where $i_{Ax} = -i_{Ay}$, $e_{Ax} = -e_{Ay} = E$, $x = 1,3,5,7$, $y = 2,4,6,9$.

When the modulation frequency of PWM is high, the carrier cycle is much smaller than the motor's electrical time constant L_s / R_s, so the influence of winding resistance can be neglected. According to (16), the current change rate of the phase winding can be obtained as

$$\frac{di_{Ax}}{dt} = \frac{U_{dc} - 2E}{2L_s}. \tag{17}$$

Assuming that the initial value of the phase current during PWM = ON is $i_{Ax}(0) = -i_{Ay}(0) = I_1$, the function expression of the phase current can be obtained as

$$i_{Ax\_ON}(t) = \frac{U_{dc} - 2E}{2L_s}t + I_1. \tag{18}$$

From Fig. 5(b), it can be observed that when PWM = OFF, current flows into the windings of phases A_1, A_3, A_5, and A_7 through the freewheeling diodes, while current flows out of the windings of phases A_2, A_4, A_6, and A_9, forming a closed circuit without passing through the negative terminal of the power supply. The winding of phase A_8 is a floating phase, with no current passing through. The corresponding voltage equation is

$$\begin{cases} u_{Ax} = 0 = R_s i_{Ax} + L_s \frac{di_{Ax}}{dt} + e_{Ax} + u_N \\ u_{Ay} = 0 = R_s i_{Ay} + L_s \frac{di_{Ay}}{dt} + e_{Ay} + u_N. \end{cases} \tag{19}$$

According to (19), the current change rate of the phase winding can be obtained as

$$\frac{di_{Ax}}{dt} = -\frac{E}{L_s}. \tag{20}$$

Since the initial value of the phase current during PWM = OFF is $i_{Ax}(dT) = -i_{Ay}(dT) = (U_{dc}–2E)dT / 2L_s + I_1$, the function expression of the phase current can be obtained as

$$i_{Ax\_OFF}(t) = -\frac{E}{L_s}t + \frac{U_{dc}}{2L_s}dT + I_1. \tag{21}$$

Based on the calculations of (18) and (21), the average value of the current within a switching cycle can be obtained as

$$I_{Ax\_mean\_8} = \frac{(2d - d^2)U_{dc} - 2E}{4L_s f} + I_1. \tag{22}$$

Furthermore, the average value of the electromagnetic torque within a switching cycle can be obtained as

$$T_{e\_mean\_8} = \frac{8E}{\omega}\left(\frac{(2d - d^2)U_{dc} - 2E}{4L_s f} + I_1\right). \tag{23}$$

The peak-to-peak value of the electromagnetic torque can be derived from the peak-to-peak value of the current within one switching cycle, as follows:

$$\Delta T_{e\_8} = \frac{8E}{\omega}\Delta I_{Ax} = \frac{4Ed(U_{dc} - 2E)}{\omega L_s f}. \tag{24}$$

According to (23) and (24), the electromagnetic torque ripple can be calculated as

$$T_{e\_rip\_8} = \frac{\Delta T_{e\_8}}{2T_{e\_mean\_8}} = \frac{d(U_{dc} - 2E)}{(2d - d^2)U_{dc} - 2E + 4L_s f I_1}. \tag{25}$$

From (25), it can be seen that the torque ripple $T_{e\_rip\_8}$ of the nine-phase BLDCM during the normal conduction period is related to the duty cycle d, the dc-bus voltage U_{dc}, the amplitude of back-EMF E, the phase inductance L_s, the switching frequency f, and the amplitude of phase current I_1.

Under steady-state load torque conditions where different conduction modes have torque output capability, if we adopt the five-phase and two-phase conduction modes, the average value of the electromagnetic torque within one switching cycle can be represented as

$$T_{e\_mean\_8} = T_{e\_mean\_5} = T_{e\_mean\_2}. \tag{26}$$

Based on the peak-to-peak value of the current within one switching cycle and the number of energized phases of the armature winding, the comparative relationship between peak-to-peak values of the electromagnetic torque can be obtained as

$$\begin{cases} \Delta T_{e\_5} = \frac{3}{5}\Delta T_{e\_8} \\ \Delta T_{e\_2} = \frac{1}{4}\Delta T_{e\_8}. \end{cases} \tag{27}$$

Furthermore, by substituting (27) into (26), we can obtain the comparative relationship of the electromagnetic torque ripple, as follows:

$$\begin{cases} T_{e\_rip\_5} = \frac{3}{5}T_{e\_rip\_8} \\ T_{e\_rip\_2} = \frac{1}{4}T_{e\_rip\_8}. \end{cases} \tag{28}$$

Based on the above analysis process, the comparative relationship of torque ripple for the m-phase BLDCM using different conduction modes can be derived, resulting in mathematical expressions, as shown in Table III.

TABLE III
TORQUE RIPPLE UNDER DIFFERENT CONDUCTION MODES AT THE SAME SPEED AND TORQUE CONDITIONS

$T_{e\_rip\_(m-1)}$	$T_{e\_rip\_(m-2)}$	$T_{e\_rip\_(m-3)}$	$T_{e\_rip\_(m-4)}$	$T_{e\_rip\_(m-5)}$
1	$\frac{4(m-5)(m-6)}{(m-2)(m-1)}$	$\frac{m-3}{m-1}$	$\frac{4(m-6)(m-7)}{(m-4)(m-1)}$	$\frac{m-5}{m-1}$

According to Table III, when $m = 9$, the torque ripple ratios of the nine-phase BLDCM under eight-phase, seven-phase, six-phase, five-phase, four-phase, three-phase, and two-phase conduction modes are 1, 0.86, 0.75, 0.6, 0.5, 0.33, and 0.25, respectively. Therefore, theoretical analysis reveals that the torque ripple caused by PWM chopping is greatest when the (m–1)-phase conduction mode is used for symmetrical multiphase BLDCM during the normal conduction period. As the number of phases generating PWM reduces, the torque ripple decreases gradually.

2) Torque Ripple During Commutation Period: As shown in Fig. 6, they are the system equivalent circuits of the nine-phase BLDCM using the eight-phase conduction mode, where Fig. 6(a) and (b), respectively, shows the current flow paths when PWM = ON and PWM = OFF within one switching cycle during the commutation period.

Taking the commutation from A_1+, A_3+, A_5+, A_7+, A_2-, A_4-, A_6-, A_9- to A_1+, A_3+, A_5+, A_8+, A_2-, A_4-, A_6-, A_9- as an example, due to the presence of inductance in the winding, the current in the switched-OFF phase A_7 does not immediately disappear, it continues to flow through the diode D_{16} for freewheeling.

From Fig. 6(a), it can be seen that when PWM = ON, current flows into the windings of phases A_1, A_3, A_5, and A_8 from the positive terminal of the power supply, while current flows out of the windings of phases A_2, A_4, A_6, and A_9, forming

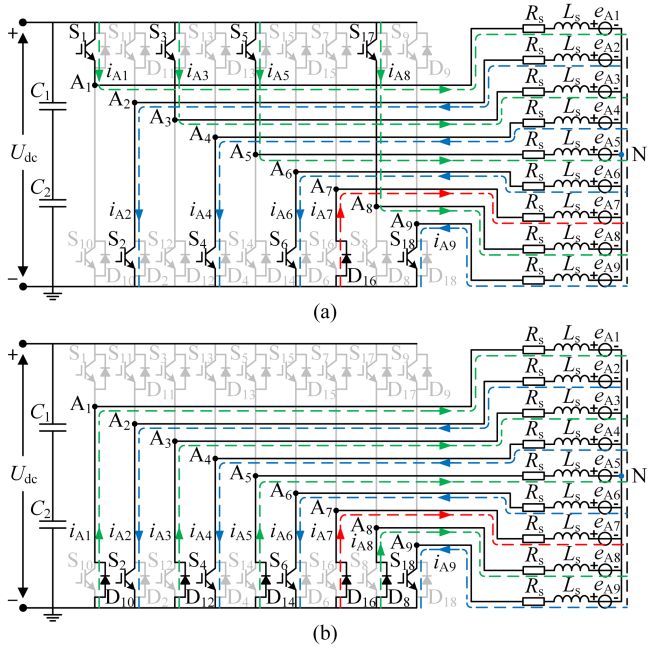

Fig. 6. System equivalent circuits of the nine-phase BLDCM with eight-phase conduction during the commutation period within one PWM cycle. (a) PWM = ON. (b) PWM = OFF.

a closed circuit through the negative terminal of the power supply. The winding of phase A_7 acts as a switched-OFF phase, with current flowing into it through the freewheeling diode. The corresponding voltage equation is

$$\begin{cases} u_{Ax} = U_{dc} = R_s i_{Ax} + L_s \frac{di_{Ax}}{dt} + e_{Ax} + u_N \\ u_{Ay} = 0 = R_s i_{Ay} + L_s \frac{di_{Ay}}{dt} + e_{Ay} + u_N \\ u_{Az} = 0 = R_s i_{Az} + L_s \frac{di_{Az}}{dt} + e_{Az} + u_N \end{cases} \tag{29}$$

where $i_{Ax} + i_{Ay} + i_{Az} = 0$, $e_{Ax} = -e_{Ay} = e_{Az} = E$, $x = 1,3,5,8$, $y = 2,4,6,9$, $z = 7$.

Assuming that the initial value of the current in the noncommutating winding A_x during PWM = ON is $i_{Ax}(0) = I_1$, according to (29), the function expression of the noncommutating current can be obtained as

$$i_{Ax\_ON}(t) = \frac{U_{dc} - 4E}{3L_s} t + I_1. \tag{30}$$

From Fig. 6(b), it can be observed that when PWM = OFF, current flows into the windings of phases A_1, A_3, A_5, and A_8 through the freewheeling diode, while current flows out of the windings of phases A_2, A_4, A_6, and A_9, forming a closed circuit without passing through the negative terminal of the power supply. The winding of phase A_7 acts as a switched-OFF phase, with current flowing into it through the freewheeling diode. The corresponding voltage equation is

$$\begin{cases} u_{Ax} = 0 = R_s i_{Ax} + L_s \frac{di_{Ax}}{dt} + e_{Ax} + u_N \\ u_{Ay} = 0 = R_s i_{Ay} + L_s \frac{di_{Ay}}{dt} + e_{Ay} + u_N \\ u_{Az} = 0 = R_s i_{Az} + L_s \frac{di_{Az}}{dt} + e_{Az} + u_N. \end{cases} \tag{31}$$

Since the initial value of the noncommutating current during PWM = OFF is $i_{Ax}(dT) = (U_{dc} - 4E)dT / 3L_s + I_1$, the function expression of the noncommutating current can be obtained as

$$i_{Ax\_OFF}(t) = -\frac{4E}{3L_s} t + \frac{U_{dc}}{3L_s} dT + I_1. \tag{32}$$

According to the calculation results of (30) and (32), the average value of the noncommutating current within one switching cycle can be obtained as

$$I_{Ax\_mean\_8} = \frac{(2d - d^2)U_{dc} - 4E}{6L_s f} + I_1. \tag{33}$$

Furthermore, based on the average and peak-to-peak values of the electromagnetic torque within one switching cycle, the expression for the torque ripple can be derived as

$$T_{e\_rip\_8} = \frac{\Delta T_{e\_8}}{2T_{e\_mean\_8}} = \frac{d(U_{dc} - 4E)}{(2d - d^2)U_{dc} - 4E + 6L_s f I_1}. \tag{34}$$

By comparing (25) and (34), it can be observed that the nine-phase BLDCM under eight-phase conduction mode exhibits a similar torque ripple expression during normal conduction and commutation periods.

Similarly, when different conduction modes are employed for control, the comparative relationship of the torque ripple can be derived based on the peak-to-peak value of the current within one switching cycle. Extending to the *m*-phase BLDCM, the torque ripple calculated during the commutation period under different conduction modes yields the same results, as shown in Table III.

The theoretical analysis above indicates that for the symmetrical winding multiphase BLDCM, reducing the number of conducting phases can decrease the torque ripple caused by PWM chopping under the same speed and steady-state load torque conditions. The variation pattern is consistent both during normal conduction and commutation periods.

B. Proposed Variable Conduction Mode Control Method

Based on the torque output characteristics of the symmetrical winding multiphase BLDCM, this article proposes a variable conduction mode control method by further analyzing the torque ripple under different conduction modes. This method can reduce torque ripple while ensuring torque output performance. Fig. 7 is a schematic diagram of the proposed method.

Specifically, in the implementation of the proposed method, the torque reference value T_{e_ref} is used to identify the torque interval, and the conduction mode is dynamically switched according to load changes. At the same time, the feedback value of the current loop is switched. In different conduction modes, the average value of all noncommutating winding currents is taken and compared with the current reference value. The difference is controlled by a single PI controller to generate the required duty cycle. The reference value of the current loop i_{ref} varies with the conduction mode and is adjusted according to their respective torque equations.

To utilize the torque reference value to identify the torque interval, the prerequisite is that the torque reference value T_{e_ref} can accurately follow the actual torque T_{e_act}. Due to the nonlinear characteristics of the motor, values calculated using the

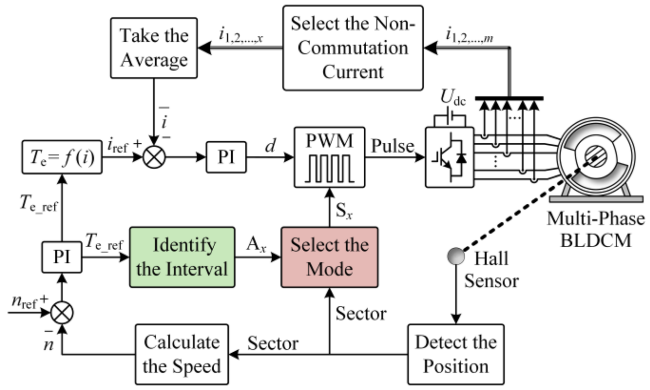

Fig. 7. Schematic diagram of the proposed variable conduction mode control method.

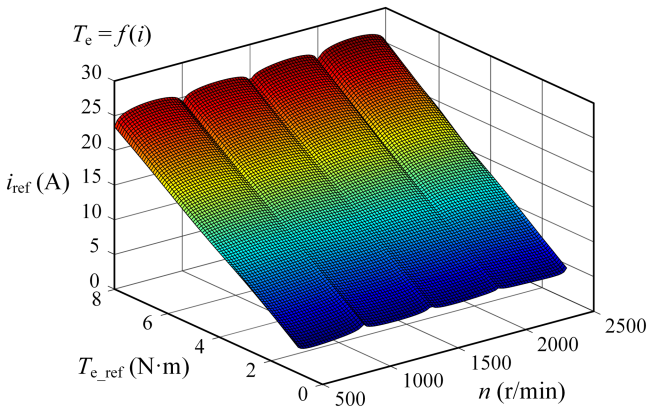

Fig. 8. Corresponding relationship between the reference torque and the reference current under different operating conditions.

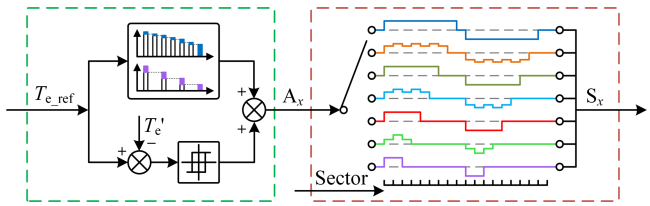

Fig. 9. Process of identifying the torque interval and selecting the conduction mode.

average torque equation are usually inaccurate. Therefore, this article uses the nine-phase BLDCM with eight-phase conduction as an example. By measuring the data under various speed and torque conditions, a correspondence relationship between the reference torque T_{e_ref} and the reference current i_{ref} is established, as shown in Fig. 8.

As shown in Fig. 9, it illustrates the process of identifying the torque interval and selecting the conduction mode. When the load torque changes dynamically, the torque interval is first identified. If the threshold conditions are met, the corresponding conduction mode is selected. If the conditions are not met, it indicates that the torque value is at the threshold boundary or fluctuating at the boundary. At this point, the difference between the torque reference value T_{e_ref} and the interval threshold T_e' is calculated. If this difference meets the hysteresis conditions set at different boundaries, a conduction mode with fewer phases is selected for control. When switching the conduction mode at any time, the conducting and floating phase windings are selected based on the rotor position sector, and the conduction rules for each mode must be preset.

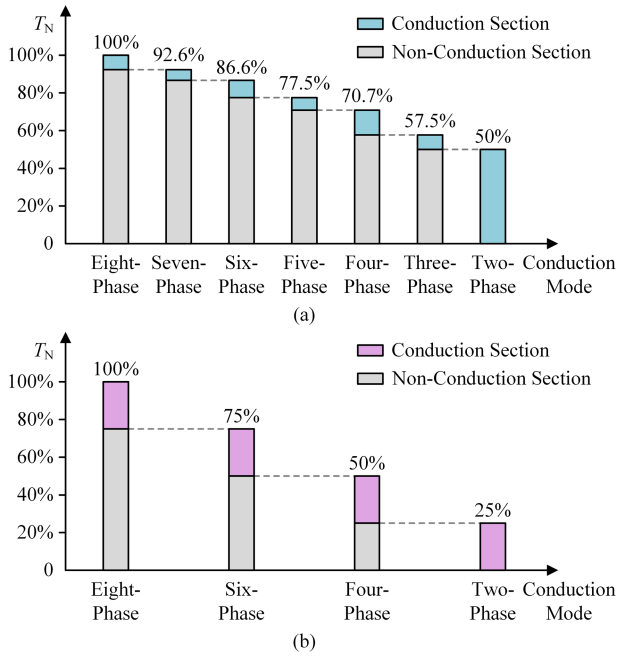

Fig. 10. Torque interval division results of the nine-phase BLDCM. (a) With equal copper loss as the constraint condition. (b) With equal phase current amplitude as the constraint condition.

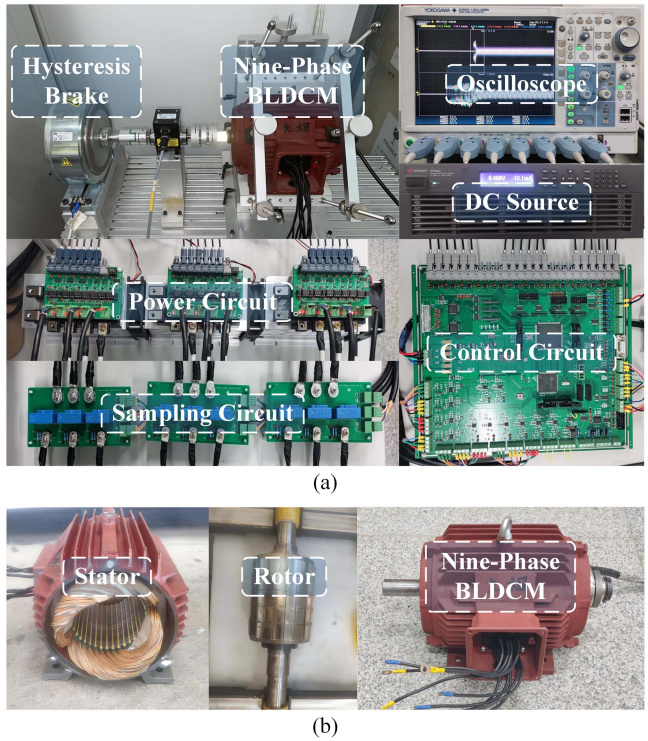

Fig. 11. Experimental platform and prototype. (a) Photographs of the experimental platform. (b) Photographs of the prototype.

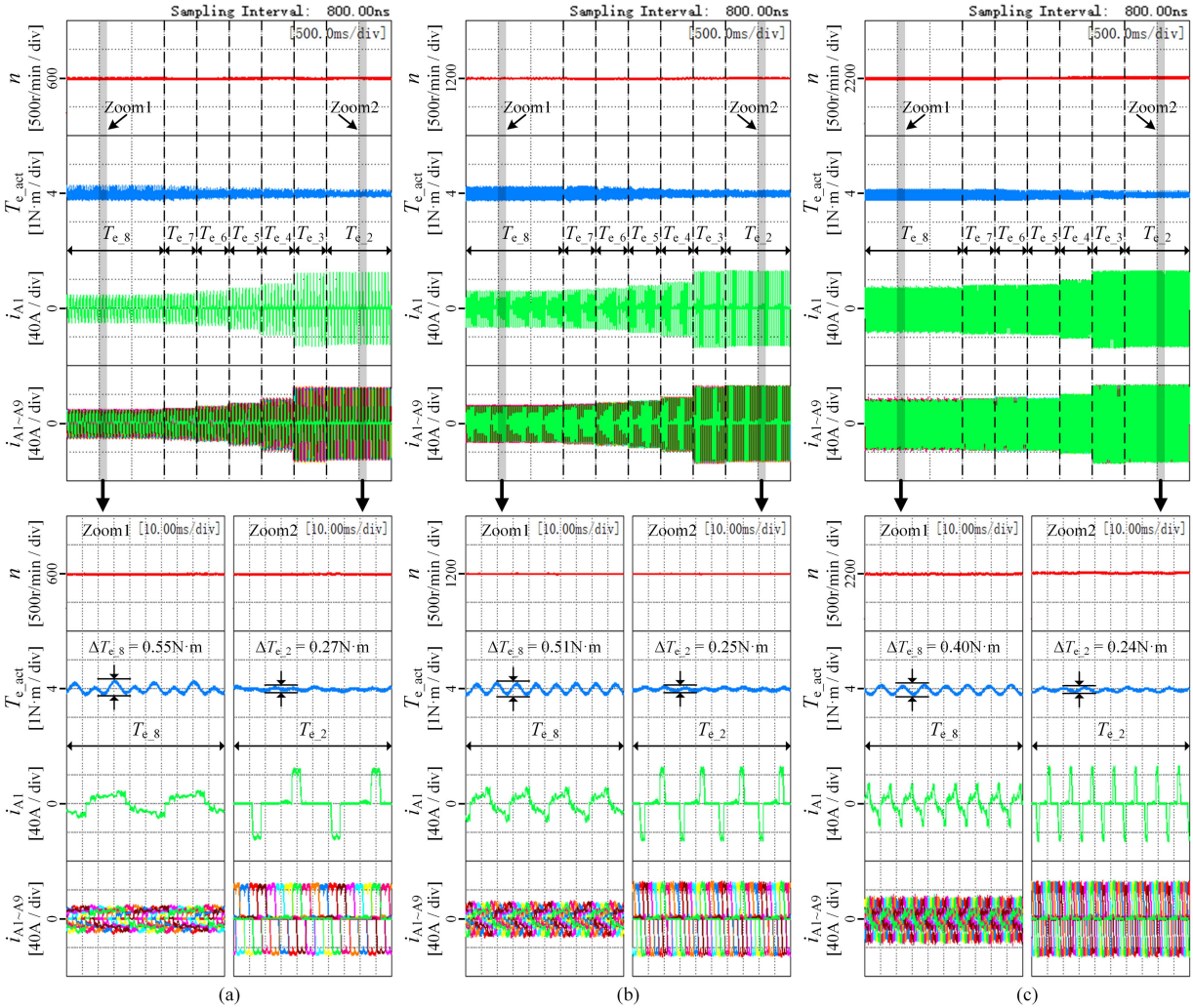

Fig. 12. Steady-state experimental results of the nine-phase BLDCM with variable conduction mode control. (a) 600 r/min. (b) 1200 r/min. (c) 2200 r/min.

When the motor operates under heavy load conditions, the load current is high, and the output power is substantial. Thus, multiphase winding conduction is used. When the motor operates under light load conditions, the load current is low, and the output power is decreased, so the number of simultaneously conducting windings is reduced. This achieves variable conduction mode control within the rated torque range.

There are no restrictions when applying the proposed method to motors with different phase numbers, but some modifications are necessary. The specific requirements for implementing the proposed method are follows.

1) For the multiphase BLDCM prototype under study, all conduction modes need to be driven individually according to winding conduction rules within a dual closed-loop control framework for speed and current.
2) Within the operating range of rated speed and rated torque, the relationship between the reference torque and reference current under each conduction mode is experimentally measured to establish an offline lookup table.
3) Based on the criteria for dividing torque intervals, specific interval thresholds are confirmed, and hysteresis conditions for the interval boundaries are determined during experimental tuning.

1) Torque Interval Division Criteria: To apply the proposed control method, the torque must be divided into intervals, with the interval thresholds serving as the switching conditions for each conduction mode. Therefore, this article proposes two criteria for dividing the torque intervals: 1) equal copper loss and 2) equal phase current amplitude as constraint conditions.

$$P_{\text{inver\_loss}} = \left(m \times U_{\text{IGBT}} \times I + m \times R_{\text{IGBT}} \times I_{\text{rms}}^2\right) \times \left(\frac{1}{2} + \frac{R_s \times I}{U_{\text{dc}}} + \frac{k_e}{U_{\text{dc}}}\sqrt{\frac{m \times k_e \times I}{k_1}}\right) + \left(m \times f \times E_{\text{total}}\right) + \left(m \times U_{\text{diode}} \times I + m \times R_{\text{diode}} \times I_{\text{rms}}^2\right) \times \left(\frac{1}{2} - \frac{R_s \times I}{U_{\text{dc}}} + \frac{k_e}{U_{\text{dc}}}\sqrt{\frac{m \times k_e \times I}{k_1}}\right). \tag{35}$$

TABLE IV
OUTPUT TORQUE OF EACH CONDUCTION MODE UNDER THE CONSTRAINT OF EQUAL COPPER LOSS

$T_{e\_(m-1)}$	$T_{e\_(m-2)}$	$T_{e\_(m-3)}$	$T_{e\_(m-4)}$	$T_{e\_(m-5)}$
T_N	$\sqrt{\frac{m-3}{m-2}}T_N$	$\sqrt{\frac{m-3}{m-1}}T_N$	$\sqrt{\frac{(m-3)(m-5)}{(m-1)(m-4)}}T_N$	$\sqrt{\frac{m-5}{m-1}}T_N$

TABLE V
OUTPUT TORQUE OF EACH CONDUCTION MODE UNDER THE CONSTRAINT OF EQUAL PHASE CURRENT AMPLITUDE

$T_{e\_(m-1)}$	$T_{e\_(m-2)}$	$T_{e\_(m-3)}$	$T_{e\_(m-4)}$	$T_{e\_(m-5)}$
T_N	$\frac{m-3}{m-1}T_N$	$\frac{m-3}{m-1}T_N$	$\frac{m-5}{m-1}T_N$	$\frac{m-5}{m-1}T_N$

The maximum output torque for each conduction mode can be obtained when using equal copper loss as a constraint condition, as shown in Table IV. Here, the maximum output torque in the (m–1)-phase conduction mode is defined as the rated load torque T_N. The torque switching points for each conduction mode can be determined based on the average torque comparison relationship shown in Table I. As shown in Fig. 10(a), it is the torque interval division results for the nine-phase BLDCM under the constraint condition of equal copper loss.

The maximum output torque for each conduction mode can be obtained when using equal phase current amplitude as a constraint condition, as shown in Table V. The torque switching points for each conduction mode can be determined based on the ratio of phase current amplitudes under the same load condition. As shown in Table V, the maximum output torque for adjacent even-phase conduction modes and odd-phase conduction modes is the same. Therefore, only the even-phase conduction modes are used for control within the rated torque range. As shown in Fig. 10(b), it is the torque interval division results for the nine-phase BLDCM under the constraint condition of equal phase current amplitude.

For the two torque interval division criteria proposed in this article, using equal copper loss as a constraint is based on the motor itself. This division ensures that the maximum loss in each conduction mode does not exceed the rated value, allowing the conduction mode with the minimal torque ripple to have a wider torque operating range. In contrast, using equal phase current amplitude as a constraint is based on the capacity of the power switching devices. This division ensures that each conduction mode's maximum phase current amplitude does not exceed the rated value, allowing each conduction mode to have the optimal torque operating range.

2) System Loss Analysis: Compared to the traditional single mode control method, using the variable conduction mode control method changes the number of conducting phases and the amplitude of phase currents, thereby altering system losses.

The losses in a motor drive system can be divided into three parts: 1) inverter losses, 2) motor losses, and 3) mechanical losses [18]. These three types of losses can be represented by (35) shown at the bottom of the this page, (36), and (37), respectively, as follows:

$$P_{\text{motor\_loss}} = \left(m \times R_s \times I_{\text{rms}}^2\right) + (k_2 \times \omega) \tag{36}$$

$$P_{\text{mech\_loss}} = k_3 \times \omega \tag{37}$$

where I and I_{rms} are the amplitude and rms value of the phase current corresponding to the current conduction mode, U_{IGBT} is the IGBT conducting voltage, R_{IGBT} is the conducting resistance, U_{diode} is the forward voltage of the freewheeling diode, R_{diode} is the forward resistance, E_{total} is the total switching losses, and k_1, k_2, k_3 are constants.

From (35), (36), and (37), we can see that both the inverter losses and motor copper losses are related to changes in phase current. In contrast, the motor iron losses and mechanical losses are unrelated, which can be simplified as functions of the mechanical angular velocity.

When a m-phase BLDCM uses variable conduction mode control, for example, when using (m–1)-phase and (m–2)-phase conduction modes, by setting (7) equal to (8), the comparative relationship of the phase current amplitudes can be derived

$$\begin{cases} \frac{I_{(m-1)}}{I_{(m-2)\_\text{up}}} = 1 \\ \frac{I_{(m-1)}}{I_{(m-2)\_\text{down}}} = \frac{m-3}{m-1}. \end{cases} \tag{38}$$

By substituting (38) into (11) and (12), the comparative relationship of the phase current rms values can be derived as

$$\begin{cases} \frac{I_{\text{rms}\_(m-1)}^2}{I_{\text{rms}\_(m-2)\_\text{up}}^2} = \frac{m-3}{m-2} \\ \frac{I_{\text{rms}\_(m-1)}^2}{I_{\text{rms}\_(m-2)\_\text{down}}^2} = \frac{m-3}{m-2}. \end{cases} \tag{39}$$

From (38) and (39), we can see that reducing the number of conducting phases in the winding will increase the phase current amplitude under the same speed and load torque conditions. Based on the corresponding current relationship, this will lead to an increase in inverter losses and motor copper losses.

Furthermore, the efficiency of the motor system can be expressed as

$$\eta = \frac{P_{\text{out}}}{P_{\text{in}}} = \frac{P_{\text{out}}}{P_{\text{out}} + P_{\text{sw}} + P_{\text{con}} + P_{\text{cu}} + P_{\text{core}} + P_{\text{mech}}} \tag{40}$$

where P_{sw} and P_{con} are the switching losses and conduction losses of the power devices, P_{cu} and P_{core} are the copper losses and iron losses of the motor, and P_{mech} is the mechanical losses. Among these, P_{sw}, P_{con}, and P_{cu} are variable losses.

The variable losses increase with the current amplitude. Therefore, when implementing the variable conduction mode control method, the system efficiency η decreases within each torque interval.

IV. EXPERIMENTAL RESULTS AND ANALYSIS

To verify the correctness of the theoretical analysis and the effectiveness of the proposed method, both steady-state and dynamic experiments are conducted on a multiphase BLDCM drive system. The experimental platform and prototype are shown in Fig. 11. The control circuit uses a DSP (TMS320F28335) and

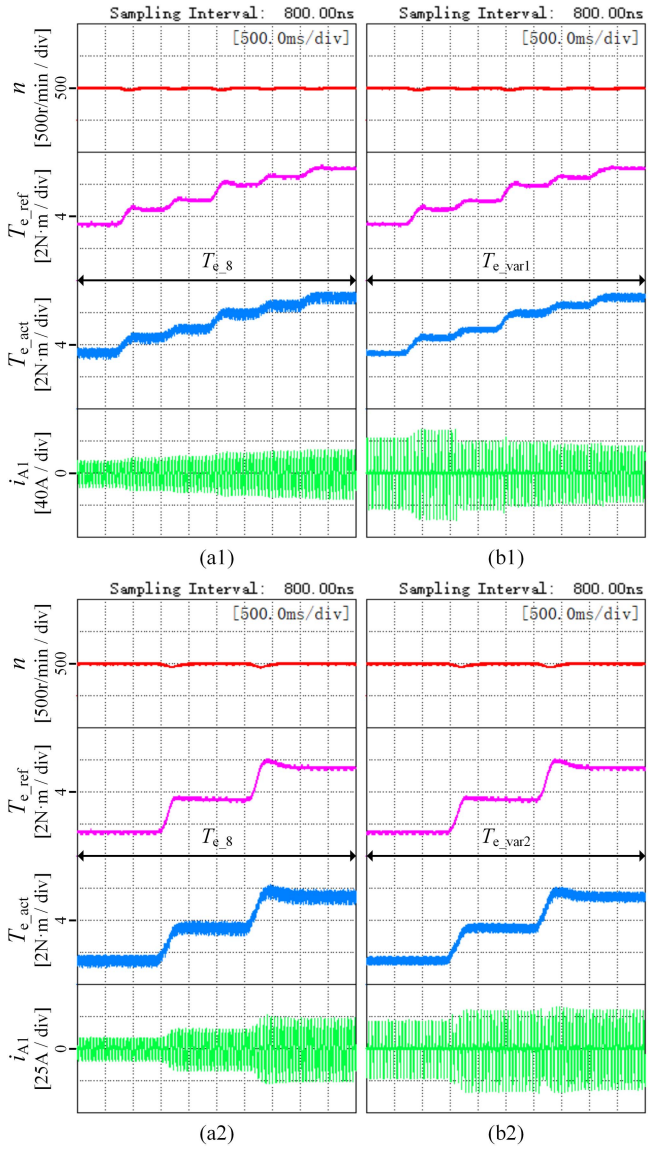

Fig. 13. Dynamic experimental results of the nine-phase BLDCM under conditions of constant speed and load step change. (a1) and (a2) Single conduction mode control. (b1) and (b2) Variable conduction mode control.

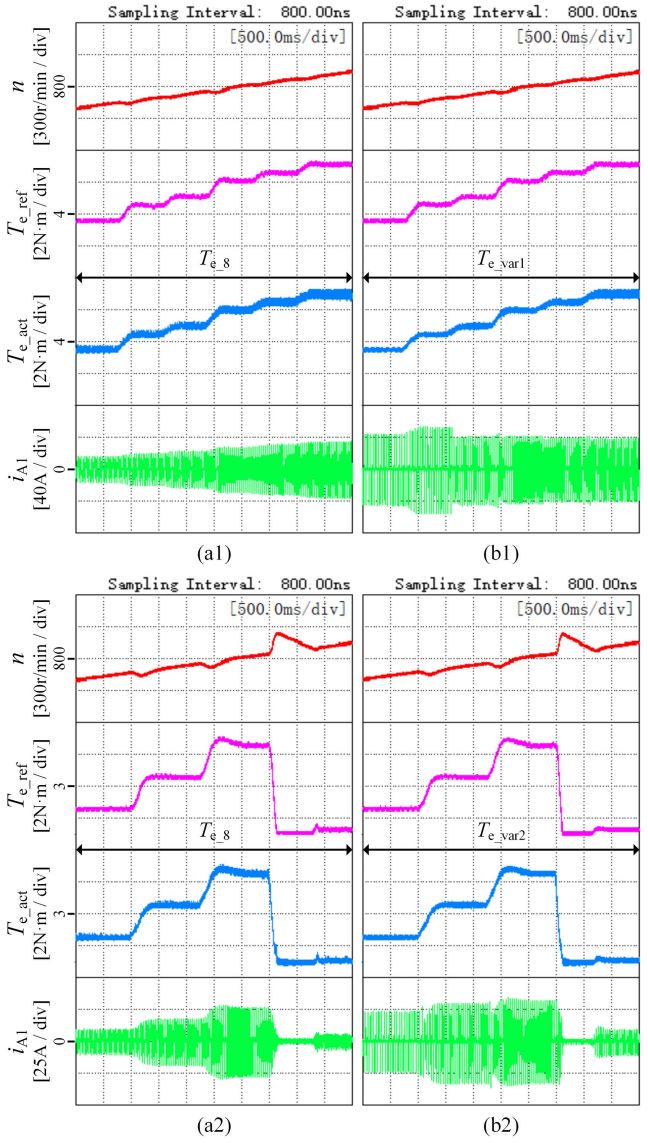

Fig. 14. Dynamic experimental results of the nine-phase BLDCM under conditions of speed change and load step change. (a1) and (a2) Single conduction mode control. (b1) and (b2) Variable conduction mode control.

an FPGA (EP1C6Q240C8) as the main control units. The power circuit employs the IPM (PM75RL1A120) as the power device and the dc source (RP7962A) as the main power supply. The sampling circuit utilizes the LEM voltage sensor (LV25-P) and LEM current sensor (LAH50-P) to collect the dc-bus voltage and the phase current. The motor is loaded using a MAGTROL hysteresis brake (AHB-12), and the actual motor torque is measured using a torque sensor (TM307). The experimental results are recorded by a Yokogawa eight-channel digital oscilloscope (DLM4058). The experimental prototype is a 2 kW nine-phase BLDCM, with the specific parameters listed in Table VI.

TABLE VI
PROTOTYPE PARAMETERS OF THE NINE-PHASE BLDCM

Parameter	Symbol	Value	Unit
Rated voltage	U_N	42.5	V
Rated power	P_N	2	kW
Rated current	I_N	23	A
Rated torque	T_N	8	N·m
Rated speed	n_N	2500	r/min
Phase resistance	R_s	0.012	Ω
Phase inductance	L_s	0.064	mH
Phase back-EMF coefficient	k_e	0.03	V/(rad/s)
Pairs of poles	p_n	2	--

A. Steady-State Experiments

To verify the feasibility of the proposed method, variable conduction mode control is applied to the nine-phase BLDCM under low-speed, medium-speed, and high-speed steady-state

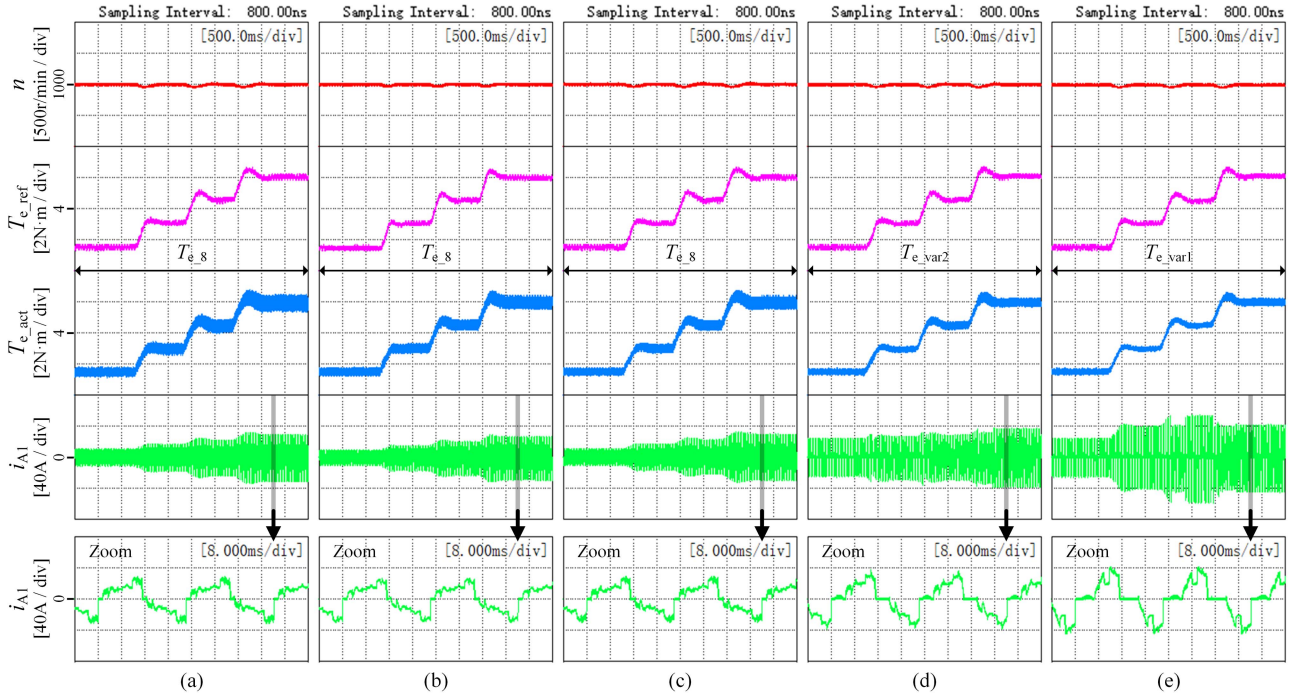

Fig. 15. Comparative experimental results of different methods. (a) Traditional method. (b) Reduction method in [12]. (c) Reduction method in [13]. (d) Proposed method under *Cons. II*. (e) Proposed method under *Cons. I*.

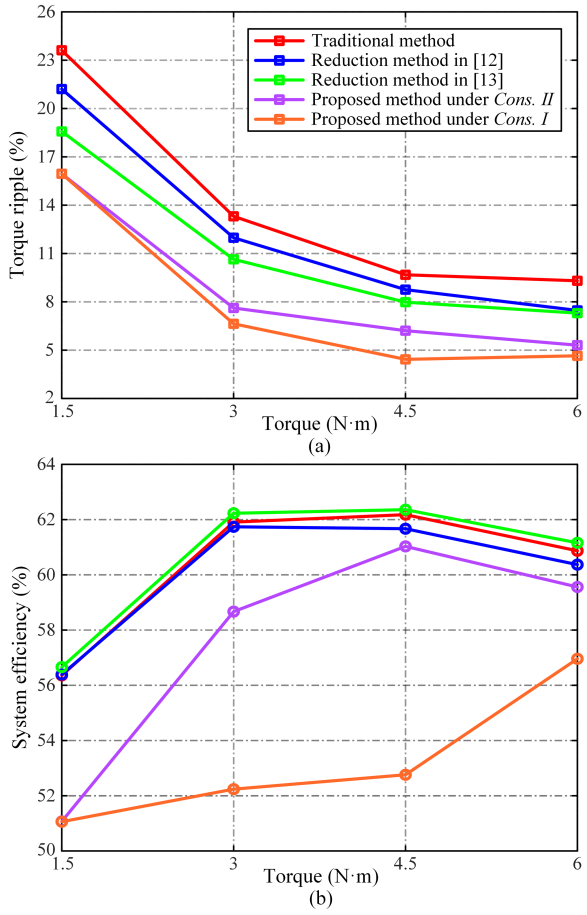

Fig. 16. Comparative experimental data of different methods. (a) Torque ripple. (b) System efficiency.

conditions. As shown in Fig. 12, these are the experimental waveforms for the nine-phase BLDCM operating at 600 r/min, 1200 r/min, and 2200 r/min with a 4 N·m load. From top to bottom, the waveforms are the speed n, the actual torque T_{e_act}, the one-phase current i_{A1}, and the nine-phase currents $i_{A1–A9}$. From left to right, the nine-phase motor successively uses eight-phase conduction, seven-phase conduction, six-phase conduction, five-phase conduction, four-phase conduction, three-phase conduction, and two-phase conduction. It should be noted that under the constraint of equal copper losses, the two-phase conduction mode can output a maximum of 4 N·m. However, under the constraint of equal phase current amplitude, the two-phase conduction mode can only output a maximum of 2 N·m.

As seen in Fig. 12, during the conduction mode switching process, the speed remains unchanged while the torque ripple gradually decreases. The conduction mode with the fewest conducting phases exhibits the smallest torque ripple. The experimental results show the same trend across different speeds. Zoom1 and Zoom2 display magnified waveforms for the eight-phase conduction and two-phase conduction modes, respectively. The peak-to-peak torque ΔT_{e_8} for the eight-phase conduction mode is 0.55 N·m, 0.51 N·m, and 0.40 N·m, while the peak-to-peak torque ΔT_{e_2} for the two-phase conduction mode is 0.27 N·m, 0.25 N·m, and 0.24 N·m. The torque ripple $T_{e\_rip\_8}$ for the eight-phase conduction mode is 6.87%, 6.37%, and 5.00%, while the torque ripple $T_{e\_rip\_2}$ for the two-phase conduction mode is 3.37%, 3.12%, and 3.00%. By comparison, the torque ripple is reduced by 3.50%, 3.25%, and 2.00%. The experimental results shown in Fig. 12 confirm the feasibility of the variable conduction mode control method. Specifically, reducing the number of conducting phases by changing the conduction mode

can decrease torque ripple under steady-state conditions with the same speed and load torque.

B. Dynamic Experiments

To verify the effectiveness of the proposed method, variable conduction mode control is applied to the nine-phase BLDCM under both steady-state and dynamic speed conditions, following the two torque interval division results described in this article.

As shown in Fig. 13, they are two sets of comparative experimental waveforms for the nine-phase BLDCM under steady-state speed with step changes in load torque. First, in Fig. 13(a1) and (b1), the torque intervals are divided based on the constraint of equal copper losses (*Cons. I*). The step changes in load torque are 3.5 N·m, 4.5 N·m, 5 N·m, 6 N·m, 6.5 N·m, and 7 N·m. Fig. 13(a1) shows that when a single conduction mode (eight-phase conduction) is applied, both torque ripple and phase current increase as the load torque. In contrast, in Fig. 13(b1), when variable conduction mode control is applied, the conduction mode can be flexibly switched within the preset torque intervals by judging whether the reference torque exceeds the interval threshold as the load torque increases. The proposed method can reduce torque ripple within the respective torque intervals compared to the single conduction mode. Second, in Fig. 13(a2) and (b2), the torque intervals are divided based on the constraint of equal phase current amplitude (*Cons. II*). The step changes in load torque are 1.5 N·m, 3.5 N·m, and 5.5 N·m. In Fig. 13(b2), when variable conduction mode control is applied, the conduction mode can be flexibly switched by identifying the changes in the reference torque, and this also reduces torque ripple within the respective torque intervals.

As shown in Fig. 14, these are two sets of comparative experimental waveforms for the nine-phase BLDCM under dynamic speed conditions with step changes in load torque. First, in Fig. 14(a1) and (b1), the torque intervals are divided based on the *Cons. I*. The experimental results are similar to the corresponding results in Fig. 13. Second, in Fig. 14(a2) and (b2), the torque intervals are divided based on the *Cons. II*. The step changes in load torque are 1.5 N·m, 3.5 N·m, 5.5 N·m, and 0 N·m. This experiment includes scenarios with sudden increases and decreases in torque. On the one hand, it verifies the effectiveness of reducing torque ripple. On the other hand, it also confirms that the proposed method has good dynamic performance.

The above two sets of experiments compare the proposed method with the traditional single mode control method. To verify the differences between the proposed method and the torque ripple reduction methods from the literature, a comprehensive comparison is conducted under the same operating conditions. As shown in Fig. 15, these are the comparison results among different methods. Fig. 15(a) is the traditional single mode control method. Fig. 15(b) is the reduction method in [12], which reduces torque ripple by increasing the switching frequency. Fig. 15(c) is the reduction method in [13], which reduces torque ripple by modifying the modulation strategy. Fig. 15(d) is the proposed method under *Cons. II*, and Fig. 15(e) is the proposed method under *Cons. I*.

In Fig. 15, the load torque step changes are 1.5 N·m, 3 N·m, 4.5 N·m, and 6 N·m. The variations in speed and reference torque remain consistent across different methods, but the torque ripple and phase current variations differ. The single mode control method in Fig. 15(a) produces the highest torque ripple. In Fig. 15(b), increasing the switching frequency from 10 kHz to 20 kHz reduces torque ripple to some extent. In Fig. 15(c), the modified modulation strategy PWM-ON-PWM also reduces torque ripple. The differences between the methods become evident when observing the changes in phase current. However, the torque ripple reduction achieved by the methods in the literature is limited. In Fig. 15(d) and (e), the proposed method, using two different torque interval division criteria for variable conduction mode control, further reduces torque ripple. Among these, Fig. 15(e) demonstrates the most effective torque ripple reduction, attributed to the use of a control mode with fewer conducting phases under this standard. These experimental results further confirm the effectiveness of the proposed method.

To quantitatively analyze the performance metrics between different methods, we recorded the experimental data from the experiments shown in Fig. 15. As illustrated in Fig. 16, this data includes torque ripple and system efficiency.

As shown in Fig. 16(a), with the increase in load torque, the torque ripple corresponding to each method gradually decreases. The traditional single mode control method exhibits the highest torque ripple, with values of 23.62%, 13.31%, 9.68%, and 9.31%. In contrast, the proposed method under *Cons. I* has the lowest torque ripple, with values of 15.95%, 6.64%, 4.43%, and 4.65%. Fig. 16(b) shows that as the load torque increases, the system efficiency for the first four methods initially increases and then decreases. The reduction method in [13] achieves the highest system efficiency, with values of 56.66%, 62.23%, 62.36%, and 61.16%. However, the proposed method under *Cons. I* has the lowest system efficiency, with values of 51.06%, 52.24%, 52.76%, and 56.96%. Compared to the methods in the literature, the proposed method results in a decrease in system efficiency. This is because, within each torque interval, it uses a control mode with fewer conducting phases, leading to an increase in phase current magnitude. This increase in inverter losses and motor copper losses causes a reduction in system efficiency when implementing the variable conduction mode control method within each torque interval.

The abovementioned experimental results indicate that in general motor systems, without increasing the hardware complexity, various performance metrics are interdependent and require balance. For example, in this study, by analyzing the torque output characteristics of a multiphase BLDCM under different conduction modes, reducing torque ripple necessitated sacrificing some system efficiency.

V. Conclusion

For the symmetrical winding multiphase BLDCM drive system, this article proposes a variable conduction mode control method, offering a new solution for low torque ripple operation in multiphase motors. This method has the following advantages.

1) The proposed method differs significantly from existing torque ripple suppression methods for the three-phase

BLDCM. It fully leverages the operational characteristics of symmetrical winding multiphase BLDCM and is a performance-optimized control strategy.

2) The proposed method is not limited to a particular phase motor. When applied to odd-phase winding multiphase BLDCM, it can be implemented with modifications according to the specific requirements of the method. This method has significant scalability.

REFERENCES

[1] W. Chen, Z. Liu, Y. Cao, X. Li, T. Shi, and C. Xia, "A position sensorless control strategy for the BLDCM based on a flux-linkage function," *IEEE Trans. Ind. Electron.*, vol. 66, no. 4, pp. 2570–2579, Apr. 2019.

[2] X. Li et al., "Low-speed rotating restart and speed recording for free-running sensorless IPMSM based on ultrahigh frequency sinusoidal wave injection," *IEEE Trans. Power Electron.*, vol. 37, no. 12, pp. 15245–15259, Dec. 2022.

[3] F. Barrero and M. J. Duran, "Recent advances in the design, modeling, and control of multiphase machines—Part I," *IEEE Trans. Ind. Electron.*, vol. 63, no. 1, pp. 449–458, Jan. 2016.

[4] M. J. Duran and F. Barrero, "Recent advances in the design, modeling, and control of multiphase machines—Part II," *IEEE Trans. Ind. Electron.*, vol. 63, no. 1, pp. 459–468, Jan. 2016.

[5] G. Wang, M. Valla, and J. Solsona, "Position sensorless permanent magnet synchronous machine drives—A review," *IEEE Trans. Ind. Electron.*, vol. 67, no. 7, pp. 5830–5842, Jul. 2020.

[6] M. Bertoluzzo, G. Buja, R. K. Keshri, and R. Menis, "Sinusoidal versus square-wave current supply of PM brushless DC drives: A convenience analysis," *IEEE Trans. Ind. Electron.*, vol. 62, no. 12, pp. 7339–7349, Dec. 2015.

[7] X. Li, C. Xia, Y. Cao, W. Chen, and T. Shi, "Commutation torque ripple reduction strategy of Z-source inverter fed brushless DC motor," *IEEE Trans. Power Electron.*, vol. 31, no. 11, pp. 7677–7690, Nov. 2016.

[8] G. Jiang, C. Xia, W. Chen, T. Shi, X. Li, and Y. Cao, "Commutation torque ripple suppression strategy for brushless DC motors with a novel noninductive boost front end," *IEEE Trans. Power Electron.*, vol. 33, no. 5, pp. 4274–4284, May 2018.

[9] Y. Cao, T. Shi, X. Li, W. Chen, and C. Xia, "A commutation torque ripple suppression strategy for brushless DC motor based on diode-assisted buck–boost inverter," *IEEE Trans. Power Electron.*, vol. 34, no. 6, pp. 5594–5605, Jun. 2019.

[10] J. Park and D.-H. Lee, "Simple commutation torque ripple reduction using PWM with compensation voltage," *IEEE Trans. Ind. Appl.*, vol. 56, no. 3, pp. 2654–2662, May/Jun. 2020.

[11] J. Lee, G. C. Lim, and J.-I. Ha, "Pulse width modulation methods for minimizing commutation torque ripples in low inductance brushless DC motor drives," *IEEE Trans. Ind. Electron.*, vol. 70, no. 5, pp. 4537–4547, May 2023.

[12] Y. Hu, C. Zhao, H. Ji, F. Ding, and Z. Jian, "Analysis of influence of frequency on torque ripple based on high-speed BLDC drive system with SiC-MOSFET," in *Proc. 22th Int. Conf. Elect. Mach. Syst.*, 2019, pp. 1–6.

[13] K. Liu, Z. Zhou, and W. Hua, "A novel region-refinement pulse width modulation method for torque ripple reduction of brushless DC motors," *IEEE Access*, vol. 7, pp. 5333–5342, 2019.

[14] J. Fang, H. Li, and B. Han, "Torque ripple reduction in BLDC torque motor with nonideal back EMF," *IEEE Trans. Power Electron.*, vol. 27, no. 11, pp. 4630–4637, Nov. 2012.

[15] T. Shi, Y. Cao, G. Jiang, X. Li, and C. Xia, "A torque control strategy for torque ripple reduction of brushless DC motor with nonideal back electromotive force," *IEEE Trans. Ind. Electron.*, vol. 64, no. 6, pp. 4423–4433, Jun. 2017.

[16] L. Zhou, T. Shi, J. Deng, W. Chen, Y. Cao, and X. Li, "Torque ripple reduction strategy for brushless DC motor based on output mode reconstruction of cuk converter," *IEEE J. Emerg. Sel. Topics Power Electron.*, vol. 11, no. 5, pp. 5244–5255, Oct. 2023.

[17] W. Chen, L. Zhu, X. Li, T. Shi, and C. Xia, "Comparing the performance of parallel multi-phase brushless DC motors: A comprehensive analysis," *IEEE Trans. Power Electron.*, vol. 38, no. 9, pp. 11290–11303, Sep. 2023.

[18] S.-W. Park, H.-S. Park, J.-J. Moon, J.-M. Kim, and W.-S. Im, "Maximum efficiency control method in 7-phase BLDC motor by changing the number of the excited phase windings," in *Proc. IEEE Energy Convers. Congr. Expo.*, 2016, pp. 1–6.

Wei Chen (Member, IEEE) was born in Shanxi, China, in 1977. He received the B.S., M.S., and Ph.D. degrees in electrical engineering from Tianjin University, Tianjin, China, in 2000, 2003, and 2006, respectively.

He is currently a Professor with the School of Electrical Engineering, Tiangong University, and the Vice President with the National Local Joint Engineering Research Center of Electric Machine System Design and Manufacturing, China. His research interests include electrical machines and drives, and power electronics.

Lixiang Zhu was born in Hebei, China, in 1997. He received the B.S. degree in electrical engineering and automation from China University of Geosciences Great Wall College, Hebei, China, in 2019, and the M.S. degree in electrical engineering in 2022 from Tiangong University, Tianjin, China, where he is currently working toward the Ph.D. degree in control science and engineering.

His research interests include electrical machines, motor drives, and power electronics.

Xinmin Li (Member, IEEE) was born in Hunan, China, in 1989. He received the B.S. degree in automation from University of Science and Technology Beijing, Beijing, China, in 2011, and the Ph.D. degree in electrical engineering from Tianjin University, Tianjin, China, in 2017.

He is currently a Professor with the School of Electrical Engineering, Tiangong University, Tianjin, China. His research interests include electrical machines and motor drives, electric drive systems of electric vehicles, power electronics, and wind power technology.

Zhiqiang Wang (Member, IEEE) was born in Tianjin, China, in 1984. He received the B.S. degree from Hebei University of Technology, Tianjin, China, in 2006, and the M.S. and Ph.D. degrees from Tianjin University, Tianjin, China, in 2008 and 2012, respectively, all in electrical engineering.

He is currently a Professor with the School of Electrical Engineering, Tiangong University, Tianjin, China. His research interests include power electronics technology and intelligent control of motor systems.

Chen Li was born in Shandong, China, in 1991. He received the B.S. degree from China University of Mining and Technology, Jiangsu, China, in 2014, and the Ph.D. degree from Tianjin University, Tianjin, China, in 2022, both in electrical engineering.

He is currently a Postdoctoral Researcher with the Zhejiang University Advanced Electrical Equipment Innovation Center, Hangzhou, China. His current research interests include electrical machines, motor drives, and power electronics.

Tingna Shi (Senior Member, IEEE) was born in Yuyao, China, in 1969. She received the B.S. and M.S. degrees from Zhejiang University, Hangzhou, China, in 1991 and 1996, respectively, and the Ph.D. degree from Tianjin University, Tianjin, China, in 2009, all in electrical engineering.

She is currently the Qiushi Distinguished Professor with the College of Electrical Engineering, Zhejiang University, Hangzhou, China. Her current research interests include electrical machines and their control systems, power electronics, and electric drives.